

# Phase-stepping algorithms for synchronous demodulation of nonlinear phase-shifted fringes

MANUEL SERVIN,<sup>\*</sup> MOISES PADILLA, IVAN CHOQUE, AND SOTERO ORDONES

*Centro de Investigaciones en Optica A. C. Loma del Bosque 115, Lomas del Campestre, 37000 Leon Guanajuato, Mexico.*

*\* [mservin@cio.mx](mailto:mservin@cio.mx)*

**Abstract:** Standard phase-stepping algorithms (PSAs) estimate the measuring phase of linear-carrier temporal-fringes with respect to a linear-reference. Linear-carrier fringes are normally obtained using feedback, closed-loop, optical phase-shifting devices. On the other hand, open-loop, phase-shifting devices, usually give fringe patterns with nonlinear phase-shifts. The Fourier spectrum of linear-carrier fringes is composed by Dirac deltas only. In contrast, nonlinear phase-shifted fringes are wideband, spread-spectrum signals. It is well known that using linear-phase reference PSA to demodulate nonlinear phase-shifted fringes, one obtains an spurious-piston. The problem with this spurious-piston, is that it may wrongly be taken as a real optical thickness. Here we mathematically find the origin of this spurious-piston and design nonlinear phase-stepping PSAs to cope with open-loop, nonlinear phase-shifted interferometric fringes. We give a general theory to tailor nonlinear phase-stepping PSAs to demodulate nonlinear phase-shifted wideband fringes.

## 1. Introduction

Linear-reference phase-shifting algorithms (PSAs) have been used to demodulate linear-carrier temporal fringes since the pioneering work by Bruning et al. [1,2]. To generate linear phase-shifting fringes one normally uses well-calibrated, feedback closed-loop, optical phase-shifters [1,2]. In contrast if one uses open-loop, phase-shifters, one normally obtain wideband, nonlinear-carrier fringes [3-9]. In these cases the PSA must also be wideband to deal with highly nonlinear phase-shifted fringes [3-9]. Hibino et al. indicated that an artifact spurious piston appears in the estimated phase when using a linear-reference PSA to demodulate nonlinear phase-shifted fringes [4-9]. This spurious-piston is a numeric artifact of the linear-reference PSA, which may be wrongly interpreted as physical optical thickness [4-9]. Real optical thickness measuring, is fundamental when testing optical material slabs in semiconductor and display equipment [4-9]. Many systematic errors have been solved in linear-carrier, linear-reference PSAs, such as phase-shift miscalibration, fringe harmonics, experiment vibrations [2-9]. For precision thickness measurement, and nonlinear phase-shifted fringes, several linear-reference PSAs with no spurious-piston have been proposed [4-9]. Recently Kim et al. have pointed-out [9] that this numerical spurious-piston has received little attention because it does not give a waving profiling error (such as detuning or harmonics) when an optical surface is profiled. However, when the central interest is to measure absolute optical thickness of transparent slabs by wavelength-tuning (for example), this numerical-piston translates into errors in thickness [4-9]. This error is given by the product of the demodulated-phase and the synthetic wavelength, which is much greater than the wavelength used [9]. Linear-reference PSAs for demodulating wideband, nonlinear-carrier fringes, have been developed using the Taylor series expansion of the arc-tangent of the phase-error [4-9]. The linear-reference PSA's coefficients are then calculated to set the first terms of this Taylor expansion to zero [4-9].

In this work we are proposing a different approach for phase demodulating temporal nonlinear-carrier fringes using wideband, synchronous, nonlinear-reference PSA. This is similar to the theory behind chirp-carrier radars [10,11]. In chirp-radars the wideband radio-

frequency (RF) pulse varies quadratically with time. When the RF chirp-pulse bounce back from the radar target, the incoming RF-signal is correlated with a synchronous, local chirp-waveform. In the case of wideband chirp-radar, one is interested in timing the amplitude of the correlation peak between the incoming RF chirp-signal and the chirped local-oscillator. Timing this correlation peak give us the round-trip target distance [10,11].

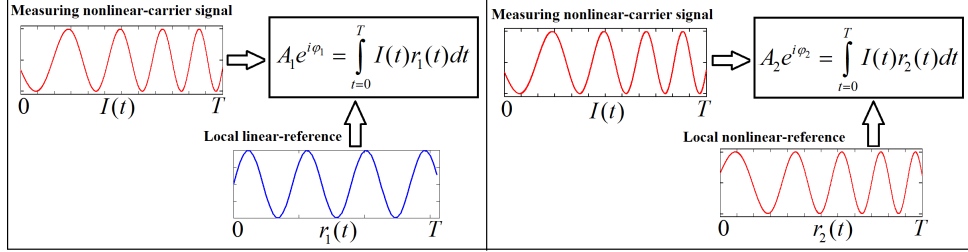


Fig.1. Schematic for linear  $r_1(t)$  and nonlinear phase-shifted reference  $r_2(t)$ . The nonlinear phase-shifted fringes is  $I(t)$ . We are showing the real part of the complex-valued reference.

As Fig. 1 shows, here we are using the same concept of synchronously following the nonlinear phase-shifted carrier fringes using the same nonlinearity phase-shifting as reference.

## 2. Linear and nonlinear phase-shifted interferometric fringes

Let us first show the usual mathematical models for linear and nonlinear phase-shifted interferometric fringes. The model for linear-carrier interferometric fringes is,

$$I_1(t) = a + b \cos(\varphi + \omega_0 t); \quad \omega_0 \in (0, \pi); \quad t \in [0, T]. \quad (1)$$

Where  $\varphi \in [-\pi, \pi]$  is the measuring phase. On the other hand, nonlinear-carrier fringes are formalized by,

$$I_2(t) = a + b \cos[\varphi + \omega_0 t + \Delta(t)]; \quad \omega_0 \in (0, \pi); \quad t \in [0, T]. \quad (2)$$

We are assuming that the nonlinearity  $\Delta(t)$  is smooth, and can be determined experimentally [3-9]. Previous papers assume that  $\Delta(t)$  can be approximated by few Taylor series terms [3,9]. Here we relax this condition, by requiring only that the derivative of  $[\omega_0 t + \Delta(t)]$  be bounded within the open interval  $(0, \pi)$ ,

$$\left[ \omega_0 + \frac{d\Delta(t)}{dt} \right] \in (0, \pi); \quad t \in [0, T]. \quad (3)$$

In Fig. 2 we show linear (in blue) and nonlinear (in red) phase-shifted fringes.

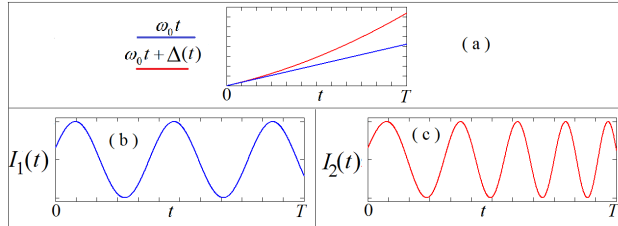


Fig. 2. Panel (a) shows in blue, linear phase-shifting, and in red, nonlinear phase-shifting. Panel (b) shows linear-carrier fringes. Panel (c) shows nonlinear-carrier fringes.

As we prove in the next sections, the nonlinear phase-shifting  $\Delta(t)$  generate a spurious-numerical piston when a linear-reference PSA is used as phase-demodulator [4-9]. Fig.2 shows an example of linear and nonlinear carrier fringes,

### 3. Fourier spectrum for linear and nonlinear phase-shifted fringes

From Eq. (1), linear fringes are single-frequency at  $\omega_0$ , having a spectrum given by [2],

$$F \left\{ a + \frac{b}{2} e^{i[\varphi + \omega_0 t]} + \frac{b}{2} e^{-i[\varphi + \omega_0 t]} \right\} = a\delta(\omega) + \frac{b}{2} e^{i\varphi} \delta(\omega - \omega_0) + \frac{b}{2} e^{-i\varphi} \delta(\omega + \omega_0). \quad (4)$$

Where  $F[\cdot]$  is the Fourier transform operator (see Fig. 3(a)). In contrast, highly nonlinear phase-shifted fringes (Eq. (2)) are wideband, and its spectrum may be modeled as,

$$F \left\{ a + \frac{b}{2} e^{i\varphi} e^{i[\omega_0 t + \Delta(t)]} + \frac{b}{2} e^{-i\varphi} e^{-i[\omega_0 t + \Delta(t)]} \right\} = a\delta(\omega) + \frac{b}{2} e^{i\varphi} C(\omega) + \frac{b}{2} e^{-i\varphi} C^*(-\omega), \quad (5)$$

Where,

$$C^*(-\omega) = F \left\{ e^{-i[\omega_0 t + \Delta(t)]} \right\}; \quad C(\omega) = F \left\{ e^{i[\omega_0 t + \Delta(t)]} \right\}. \quad (6)$$

Figure 3 shows schematically the spectrum of linear and wideband nonlinear-carrier fringes. In Eq. (5) the terms  $C^*(-\omega)$  and  $C(\omega)$  are wideband spectra.

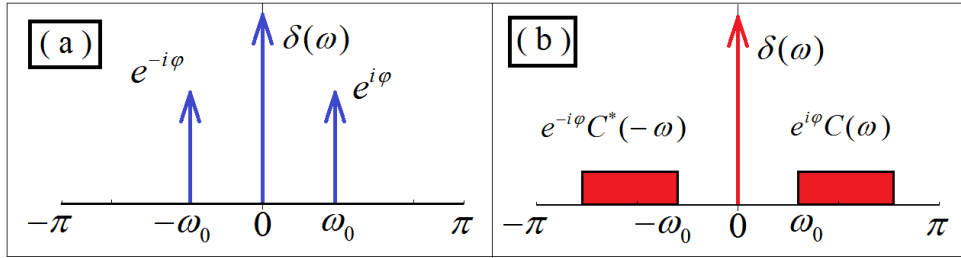


Fig. 3. Panel (a) shows the three delta-spectrum of linear-carrier fringes, and in panel (b) the wideband spectrum of nonlinear phase-shifted fringes.

Summarizing, linear-phase carrier fringes have a three delta spectrum (Fig 3(a)); while nonlinear-phase carrier fringes have two spread-spectrum components (Fig. 3(b)).

### 4. Linear and nonlinear reference PSAs

Let us now show the mathematical form of phase-shifting algorithms (PSAs) using linear and nonlinear-reference for demodulating nonlinear-carrier fringes

#### 3.1 Standard linear-reference PSA for demodulating linear-carrier fringes

The general form for standard linear-carrier, linear-reference PSA is [2],

$$Ae^{i\varphi} = \sum_{n=0}^{N-1} \overbrace{[c_n e^{i\omega_0 n}]}^{\text{Linear Reference}} \overbrace{[a + b \cos(\varphi + \omega_0 n)]}^{\text{Linear Carrier Fringes}}. \quad (7)$$

These are the standard linear-carrier, linear-reference PSAs in use since 1974 [1,2].

#### 3.2 Linear-reference PSA for demodulating nonlinear-carrier fringes

People has proposed linear-reference PSAs to demodulate nonlinear-carrier fringes as [3-9],

$$A_1 e^{i(\varphi + Piston)} = \sum_{n=0}^{N-1} \overbrace{\left[ d_n e^{i \omega_0 n} \right]}^{\text{Linear Reference}} \overbrace{\left[ a + b \cos(\varphi + \omega_0 n + \Delta(n)) \right]}^{\text{Nonlinear Carrier Fringes}}. \quad (8)$$

As we show next, using a linear-reference PSA, we generally obtain a spurious-piston,  $Piston \neq 0$  [4-9]. Hibino et al., have proposed linear-reference PSAs to eliminate this spurious piston [4-9]. Here we are proposing an alternative solution, a more natural way (we believe), for disappearing this non-desired, spurious-piston.

### 3.3 Nonlinear-reference PSA for demodulating nonlinear-carrier fringes

We specifically propose the use of a nonlinear-reference PSA which has the following form,

$$A_2 e^{i\varphi} = \sum_{n=0}^{N-1} \overbrace{\left[ w_n e^{i[\omega_0 n + \Delta(n)]} \right]}^{\text{Nonlinear Reference}} \overbrace{\left[ a + b \cos(\varphi + \omega_0 n + \Delta(n)) \right]}^{\text{Nonlinear Carrier Fringes}}; \quad (w_n \in \mathbb{R}). \quad (9)$$

Note that the nonlinear-reference  $\exp[i(\omega_0 n + \Delta(n))]$  is synchronous with the nonlinear-carrier  $\cos[\varphi + \omega_0 n + \Delta(n)]$ ; this fact makes the spurious-piston disappear  $Piston=0$ . The weighting coefficients ( $w_n$ ) are chosen to approximate a Hilbert quadrature filter.

## 5. Spurious-piston using linear phase-shifted reference PSAs

Using a linear-reference PSAs to demodulate nonlinear-carrier fringes (Eq. (8)) one obtains,

$$A_1 e^{i[\varphi + Piston]} = \sum_{n=0}^{N-1} d_n e^{-i \omega_0 n} I_2(n) = \sum_{n=0}^{N-1} \left\{ a + \frac{b}{2} e^{i\varphi} e^{i[\omega_0 n + \Delta(n)]} + \frac{b}{2} e^{-i\varphi} e^{-i[\omega_0 n + \Delta(n)]} \right\} d_n e^{-i \omega_0 n} \quad (10)$$

Performing the indicated multiplications one obtains,

$$A_1 e^{i[\varphi + Piston]} = a \left[ \sum_{n=0}^{N-1} d_n e^{-i \omega_0 n} \right] + \frac{b}{2} e^{i\varphi} \left\{ \sum_{n=0}^{N-1} d_n e^{i\Delta(n)} \right\} + \frac{b}{2} e^{-i\varphi} \left[ \sum_{n=0}^{N-1} d_n e^{-i[2\omega_0 n + \Delta(n)]} \right] \quad (11)$$

The coefficients  $d_n$  are chosen such that the first and third square-brackets are set to zero as,

$$\left[ \sum_{n=0}^{N-1} d_n e^{-i \omega_0 n} \right] = 0, \quad \text{and} \quad \left[ \sum_{n=0}^{N-1} d_n e^{-i[2\omega_0 n + \Delta(n)]} \right] = 0. \quad (12)$$

Obtaining the desired analytic signal as,

$$A_1 e^{i(\varphi + Piston)} = \frac{b}{2} e^{i\varphi} \left\{ \sum_{n=0}^{N-1} d_n e^{i\Delta(n)} \right\}; \quad Piston = \arg \left\{ \sum_{n=0}^{N-1} d_n e^{i\Delta(n)} \right\}. \quad (13)$$

As we see, in general, the spurious-piston is non-zero ( $Piston \neq 0$ ), and it may give erroneous absolute optical thickness measurements [4-9].

## 6. No spurious-piston using nonlinear phase-shifted reference PSA

Now using a synchronous (matched-phase) nonlinear reference PSA (Eq. (9)) one gets,

$$A_2 e^{i\varphi} = \sum_{n=0}^{N-1} w_n e^{-i[\omega_0 n + \Delta(n)]} I_2(n) = \sum_{n=0}^{N-1} \left[ a + \frac{b}{2} e^{i\varphi} e^{i[\omega_0 n + \Delta(n)]} + \frac{b}{2} e^{-i\varphi} e^{-i[\omega_0 n + \Delta(n)]} \right] w_n e^{-i[\omega_0 n + \Delta(n)]} \quad (14)$$

Performing the multiplications one obtains,

$$A_2 e^{i\varphi} = a \left[ \sum_{n=0}^{N-1} w_n e^{-i[\omega_0 n + \Delta(n)]} \right] + \frac{b}{2} e^{i\varphi} \left[ \sum_{n=0}^{N-1} w_n \right] + \frac{b}{2} e^{-i\varphi} \left[ \sum_{n=0}^{N-1} w_n e^{-i[2\omega_0 n + \Delta(n)]} \right] \quad (15)$$

As we did before, to obtain just the desired analytic-signal  $\exp[i\varphi]$  one needs,

$$\left[ \sum_{n=0}^{N-1} w_n e^{-i[\omega_0 n + \Delta(n)]} \right] = 0; \quad \text{and} \quad \left[ \sum_{n=0}^{N-1} w_n e^{-i[2\omega_0 n + \Delta(n)]} \right] = 0. \quad (16)$$

Obtaining the phase-demodulated signal  $Ae^{i\varphi}$  as,

$$A_2 e^{i\varphi} = \frac{b}{2} e^{i\varphi} \sum_{n=0}^{N-1} w_n; \quad (w_n \in \mathbb{R}). \quad (17)$$

The spurious piston has naturally disappeared ( $Piston=0$ ) thanks to the use of a synchronous nonlinear-reference  $\exp\{-i[\omega_0 n + \Delta(n)]\}$  in the PSA.

## 7. Spectral design for nonlinearly phase-shifted reference PSAs

In previous section we gave an algebraic approach for calculating the coefficients ( $w_n \in \mathbb{R}$ ) for nonlinear phase-shifted reference PSAs. Here we develop a more intuitive spectral design. The impulse response of the nonlinear reference PSA (Eq. (9)) is.

$$h_2(t) = \sum_{n=0}^{N-1} w_n e^{i[\omega_0 n + \Delta(n)]} \delta(t-n); \quad (w_n \in \mathbb{R}). \quad (18)$$

Then its FTF is  $H_2(\omega) = F[h_2(t)]$ ,

$$H_2(\omega) = F \left\{ \sum_{n=0}^{N-1} w_n e^{i[\omega_0 n + \Delta(n)]} \delta(t-n) \right\} = \sum_{n=0}^{N-1} w_n e^{i[\omega_0 n + \Delta(n)]} e^{-in\omega}. \quad (19)$$

The coefficients ( $w_n$ ) of  $H_2(\omega)$  are chosen to fulfill with the wideband conditions,

$$\begin{aligned} H_2(\omega) &= 0 \quad \text{for} \quad \omega \in [-\pi, 0] \\ H_2(\omega) &\neq 0 \quad \text{for} \quad \omega \in (0, \pi) \end{aligned} \quad (20)$$

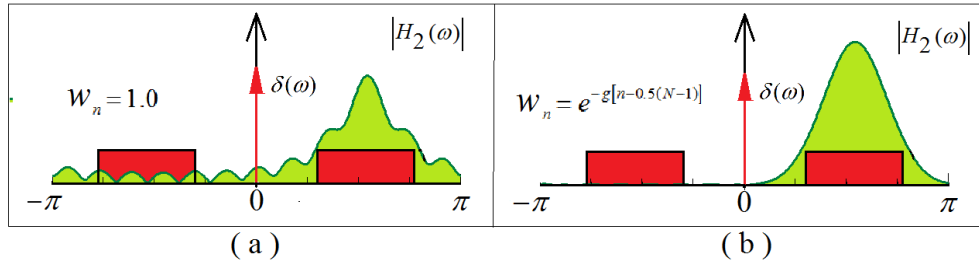


Fig. 4. Two nonlinear-reference PSA, FTF-spectra. Panel (a) shows (in green) the FTF of a square-window, nonlinear-reference PSA. Panel (b) shows the FTF of a nonlinear-reference PSA with Gaussian window [12,13]. In red we show the wideband spectrum of the nonlinear-carrier fringes. The FTF in panel (b) is a smooth approximation of a Hilbert quadrature filter.

As Fig. 4(a) shows  $H_2(\omega)$  for a square-window ( $w_n = 1.0$ ). We can see that  $H_2(\omega)$  is not zero for  $\omega \in [-\pi, 0]$ , obtaining an erroneous phase. One solution to this is to use an apodizing window [12,13]. We used a Gaussian window  $w_n = e^{-g[n-0.5(N-1)]^2}$ ; ( $g < 1.0$ ), and its FTF  $H_2(\omega) = F[h_2(t)]$  is shown in Fig. 4(b). Of course other weightings windows ( $w_n \neq 1$ ) may be used [12,13].

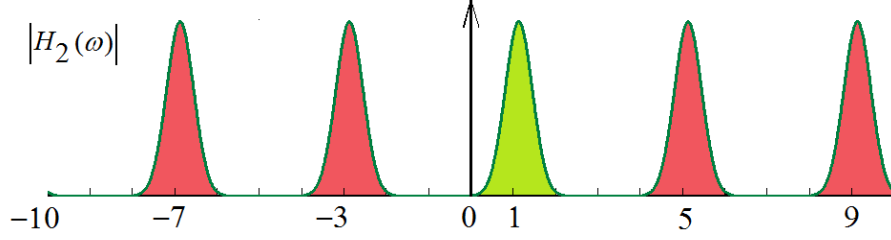


Fig. 5. Fundamental (in green) and harmonic (in red) FTF response for the nonlinear-reference PSA. As usual the harmonics  $\{-7,-3,5,9\}$  response is asymmetrical.

In Fig. 5 we show the (normalized frequency) harmonic response of the apodized, nonlinear reference PSA.

### 8. Signal-to-noise ratio (SNR) for linear and nonlinear reference PSA

Here we find the SNR [2] of the phase-demodulated nonlinear-carrier fringes corrupted by additive white Gaussian-noise (AWGN). The noisy fringes are,

$$I_2(t) = \sum_{n=0}^{N-1} \{ a + b \cos[\varphi + \omega_0 t + \Delta(t)] + N(t) \} \delta(t - n). \quad (21)$$

Where the noise spectral density  $S(\omega)$  is flat, and it is given by,

$$S(\omega) = F[R_{NN}(\tau)] = F[E\{N(t)N(t+\tau)\}] = \frac{N_0}{2}; \quad \omega \in [-\pi, \pi]. \quad (22)$$

Being  $R_{NN}(\tau) = E\{N(t)N(t+\tau)\}$  the ensemble autocorrelation function of  $N(t)$  [2]. The flat noise power-spectrum of  $N(t)$  is modified to  $(N_0/2)|H_2(\omega)|^2$  [2].

For nonlinear-carrier fringes, and linear-reference PSA, the SNR is given by,

$$\text{SNR}_1 = \frac{\text{Signal Energy}}{\text{Noise Energy}} = \frac{\left(\frac{b}{2}\right)^2 \left| \sum_{n=0}^{N-1} d_n e^{-i\Delta(n)} \right|^2}{\left(\frac{N_0}{2}\right) \int_{-\pi}^{\pi} |H_1(\omega)|^2 d\omega}. \quad (23)$$

On the other hand for nonlinear-carrier and reference, the SNR is given,

$$\text{SNR}_2 = \frac{\text{Signal Energy}}{\text{Noise Energy}} = \frac{\left(\frac{b}{2}\right)^2 \left| \sum_{n=0}^{N-1} w_n \right|^2}{\left(\frac{N_0}{2}\right) \int_{-\pi}^{\pi} |H_2(\omega)|^2 d\omega}. \quad (24)$$

Where  $(N_0/2) \int |H_1(\omega)|^2 d\omega$ , and  $(N_0/2) \int |H_2(\omega)|^2 d\omega$  are the total filtered-noise energy. The energy of  $A_2 e^{i\varphi}$  using the nonlinear-reference PSA is generally higher than the energy of  $A_1 e^{i[\varphi + \text{Piston}]}$  using a linear-reference PSA, this is because,

$$\left(\frac{b}{2}\right)^2 \left| \sum_{n=0}^{N-1} w_n \right|^2 \geq \left(\frac{b}{2}\right)^2 \left| \sum_{n=0}^{N-1} d_n e^{-i\Delta(n)} \right|^2. \quad (25)$$

Assuming that both have about the same bandwidth  $|H_1(\omega)| \approx |H_2(\omega)|$ , one obtains,

$$\text{SNR}_2 \geq \text{SNR}_1. \quad (26)$$

As conclusion, the SNR is generally higher for a PSA with nonlinear-reference.

### 9. Example of a 13-steps Gaussian-window nonlinear-reference PSA

Here we are given a computer simulation example of a 13-step nonlinear-reference PSA applied to nonlinear-carrier fringes. The most usual phase-shifted nonlinearity is quadratic,  $\Delta(n) = \varepsilon_2 n^2$  [3-9]. We start by considering nonlinear-carrier fringes as,

$$I(t; \varphi) = \sum_{n=0}^{12} [1 + \cos(\varphi + \omega_0 n + \varepsilon_2 n^2)] \delta(t - n); \quad (\omega_0 = 0.35\pi, \varepsilon_2 = 0.05\omega_0). \quad (27)$$

The non-linear phase and the interferometric chirp-waveform is shown in Fig. 6.

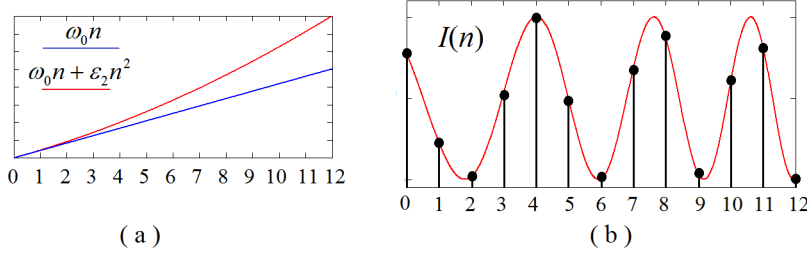


Fig. 6. Panel (a) shows the linear (in blue) and a strong nonlinear, quadratic-carrier (in red). Panel (b) shows the chirp-carrier fringes sampled at a constant sampling rate.

The specific form of the 13-steps nonlinear, chirp-reference PSA is given by,

$$A_2 e^{i\varphi} = \sum_{n=0}^{12} w_n e^{i[\omega_0 n + \varepsilon_2 n^2]} I(n; \varphi); \quad w_n = e^{-0.1[n - 0.5(N-1)]^2}. \quad (28)$$

We have assumed no linear detuning. The PSA reference  $\exp\{-i[\omega_0 n + \varepsilon_2 n^2]\}$ , is synchronous with the chirp-fringes. The FTF ( $H_2(\omega)$ ) of the nonlinear-reference PSA is,

$$H_2(\omega) = F[h_2(t)] = F\left[\sum_{n=0}^{12} w_n e^{i[\omega_0 n + \varepsilon_2 n^2]} \delta(t - n)\right] = \sum_{n=0}^{12} w_n e^{i[\omega_0 n + \varepsilon_2 n^2]} e^{-in\omega}. \quad (29)$$

And its temporal and spectral graphs are shown in Fig. 7.

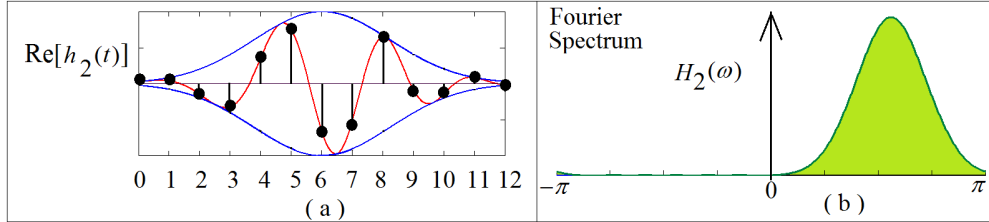


Fig. 7. Panel (a) shows the real component of the complex-valued chirp-wavelet impulse response. In panel (b) we show the PSA-FTF of the chirp-wavelet impulse response. The weighting coefficients shape the FTF as a smooth approximation of a Hilbert quadrature filter.

Next Fig. 8 shows, superimposed, the fringe-data and the chirp-reference PSA spectra.

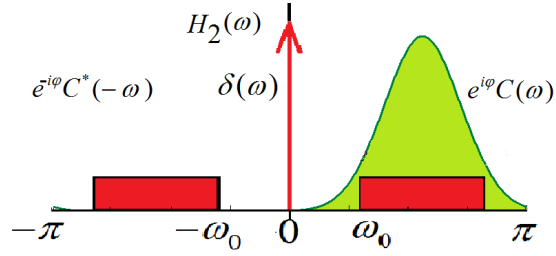


Fig. 8. Superimposed nonlinear fringe spectrum (in red), and FTF of the Gaussian-window, nonlinear-reference PSA (in green). This FTF has negligible response at the negative frequencies of the wideband fringes. This FTF approximates a Hilbert quadrature filter.

We evaluate our nonlinear-reference PSA demodulation error by the following formula,

$$\varphi_{Error} = \varphi - \arg \left[ \sum_{n=0}^{12} w_n e^{i(\omega_0 n + \varepsilon_2 n^2)} I(n; \varphi) \right]; \quad \varphi \in [0, 2\pi]. \quad (30)$$

Finally Fig. 9 shows the phase estimation error  $\varphi_{Error}$ , for  $\varphi \in [0, 2\pi]$ .

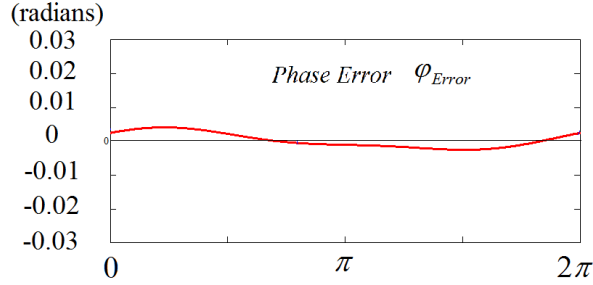


Fig. 9 Phase error given by Eq. (32). Note the vertical scale is within  $[-0.03, 0.03]$  radians.

Figure 9 shows that the peak phase demodulation error  $\varphi_{Error}$  is about 0.04 radians.

## 10. Example of a 13-steps square-window nonlinear-reference PSA

Here we analyze a square-window nonlinear-reference PSA for the same fringes used in previous section  $\Delta(n) = \varepsilon_2 n^2$ . Then our square-window PSA is,

$$A_2 e^{i\varphi_{Square}} = \sum_{n=0}^{12} w_n e^{i[\omega_0 n + \varepsilon_2 n^2]} \{1 + \cos[\varphi + \omega_0 n + \varepsilon_2 n^2]\}; \quad w_n = 1.0. \quad (31)$$

The spectral graph of the FTF associated to this PSA is shown in Fig. 10.

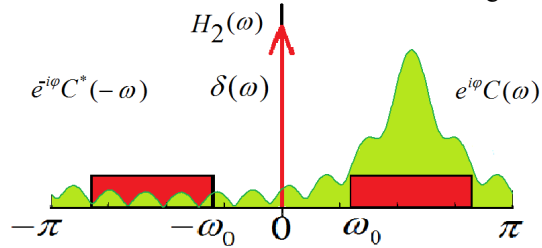


Fig. 10. Spectral response (FTF) for the square-window, nonlinear-reference PSA. This square window cannot be used because it has large response in the origin and the left side of the fringe spectrum. This FTF is a bad approximation of a one-sided Hilbert quadrature filter.



As Fig. 11 shows, the DC background of the fringes is not fully filtered-out, and also large energy from the unwanted conjugate-signal leaks into the desired analytic signal.

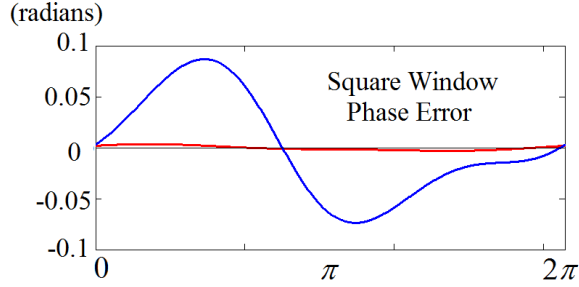


Fig. 11. The blue trace shows the phase-error for the 13-step, square-window, nonlinear-reference PSA. For comparison, the red-trace is the phase error corresponding to the Gaussian window seen in previous section. Note that the vertical scale is now  $[-0.1, 0.1]$  radians.

Figure 11 shows in the blue trace the phase-error of the square-window nonlinear-reference PSA. We summarize this section by remarking the fact that synchronously following the nonlinear-carrier variations of the fringes is not enough. One must also apply an apodizing weighting window to the nonlinear-reference PSA [12,13].

## 11. Discussion of the proposed nonlinear-reference PSA theory

Before our general summary, we want to make a clear wrap-up of our contribution. The basic theory presented herein is completely general. The only restriction is that the nonlinear-carrier fringe spectrum be bandlimited. For the readers' convenience we rewrite the few equations required. The nonlinear-carrier fringes are modeled as,

$$I_2(t) = a + b \cos[\varphi + \omega_0 t + \Delta(t)]; \quad t \in [0, T]; \quad \omega_0 \in (0, \pi). \quad (32)$$

Where the *only* restriction about the phase-shifted variation  $[\omega_0 t + \Delta(t)]$  is,

$$\left[ \omega_0 + \frac{d\Delta(t)}{dt} \right] \in (0, \pi) ; \quad t \in [0, T] . \quad (33)$$

This restriction on  $\Delta(t)$  is more general to previous efforts which assumed that  $\Delta(t)$  should be expansible as a Taylor series [3-9]. We then proposed our nonlinear-reference PSA as,

$$A_2 e^{i\varphi} = \sum_{n=0}^{N-1} w_n e^{i[\omega_0 n + \Delta(n)]} I_2(n); \quad (w_n \in \mathbb{R}). \quad (34)$$

The window  $(w_n)$  shape the FTF of this PSA, and it may be taken from a wide set of functions [12,13]. This analytic signal has no spurious piston. The FTF of this PSA is,

$$H_2(\omega) = F[h_2(t)] = F \left\{ \sum_{n=0}^{N-1} w_n e^{i[\omega_0 n + \Delta(n)]} \delta(t-n) \right\} = \sum_{n=0}^{N-1} w_n e^{i[\omega_0 n + \Delta(n)]} e^{-in\omega} . \quad (35)$$

The coefficients  $(w_n)$  shape this FTF to cover the right hand-side spectrum of the fringes as,

$$\begin{aligned} H_2(\omega) &= 0 \quad \text{for } \omega \in [-\pi, 0] \\ H_2(\omega) &\neq 0 \quad \text{for } \omega \in (0, \pi) \end{aligned} \quad (36)$$

These five equations succinctly show our theory for designing nonlinear-reference PSAs for phase-demodulating nonlinear-carrier fringes without spurious-piston.

## 12. Summary

Here we have given a frequency transfer function (FTF) approach for designing nonlinear phase-shifting algorithms (PSAs) applied to demodulate nonlinear phase-shifted fringes. The estimated nonlinear phase-step variations of the fringes [4-9], constitute also our nonlinear phase-step reference for the PSA. We then find the real-valued PSA coefficients ( $w_n$ ) that shapes the FTF spectrum of the PSA. The spectral shape of the nonlinear reference PSA smoothly approximate a Hilbert quadrature filter. As such, the spectral FTF shaping must render almost zero the left side (including zero) of the fringes spectrum.

Phase-demodulation of nonlinear phase-shifted fringes using linear-reference PSAs has been studied before [3-9]. As mentioned, in general, linear-reference PSAs obtain an artifact, numeric piston when demodulating nonlinear-carrier fringes [4-9]. This spurious-piston may render the phase measurement of absolute optical thickness erroneous [4-9]. Hibino et al have eliminated this spurious-piston by imposing some conditions on the coefficients of linear-reference PSAs [4-9]. Here we have seen that using a nonlinear-reference PSA synchronous with the nonlinear-carrier fringes, the spurious piston disappears in a more natural way (we believe). We think that our nonlinear-phase reference PSA approach shed new light for understanding temporal phase-demodulation of broadband interferometric fringes.

## References

1. J. H. Bruning, D. R. Herriott, J. E. Gallagher, D. P. Rosenfeld, A. D. White, and D. J. Brangaccio, "Digital wavefront measuring interferometer for testing optical surfaces and lenses," *Appl. Opt.* 13(11), 2693-2703 (1974).
2. M. Servin, A. Quiroga, and Moises Padilla, *Fringe Pattern Analysis for Optical Metrology, Theory Algorithms and Applications*, Wiley-VCH, Verlag GmbH&Co. Weinhand Germany (2014).
3. Chiayu Ai and James C. Wyant, "Effect of piezoelectric transducer nonlinearity on phase shift interferometry," *Appl. Opt.* 26(6), 1112-1116 (1987).
4. K. Hibino, B. F. Oreb, D. I. Farrant, and K. G. Larkin, "Phase-shifting algorithms for nonlinear and spatially nonuniform phase shifts," *J. Opt. Soc. Am. A* 14(4), 918-930 (1997).
5. K. Hibino, "Error Compensating Phase Measuring Algorithms in a Fizeau Interferometer," *Opt. Rev.*, 6(6) 529-538 (1999).
6. K. Hibino, B. F. Oreb, and P. S. Fairman, "Wavelength-scanning interferometry of a transparent parallel plate with refractive-index dispersion," *Appl. Opt.* 42(19) 3888-2895 (2003)
7. Y. Kim, K. Hibino, R. Hanayama, N. Sugita, and M. Mitsuishi, "Multiple-surface interferometry of highly reflective wafer by wavelength tuning," *Opt. Exp.*, 22(18) 21145-21156 (2014).
8. Y. Kim, K. Hibino, N. Sugita, and M. Mitsuishi, "Absolute optical thickness measurement of transparent plate using excess fraction method and wavelength-tuning Fizeau interferometer," *Opt. Express* 23(4), 4065-4073 (2015).
9. Y. Kim, K. Hibino, and M. Mitsuishi, "Interferometric profile measurement of optical-thickness by wavelength tuning with suppression of spatially uniform error," *Opt. Express* 26(8), 10870-10878 (2018).
10. J. R. Klauder, A. C. Price, S. Darlington, W. J. Albersheim, "The theory and design of chirp radars", *Bell Svs. Tech. J.*, 39, 745-808 (1960).
11. R. Millet, "A matched-filter pulse-compression system using a nonlinear FM waveform," *IEEE trans. on aero. and elect.*, 6(1) 73-78 (1970).
12. F. J. Harris, "On the use of windows for harmonic analysis with the discrete Fourier transforms," *Proc. IEEE* 66(1), 51-83 (1978).
13. P. de Groot, "Derivation of algorithms for phase-shifting interferometry using the concept of a data-sampling window," *Appl. Opt.* 34(22),4723-4730 (1995).